Journal of Engg. Research Vol.10 No. (1A) pp. 113-130 DOI: 10.36909/jer.9633

A hybrid digital image watermarking scheme incorporating DWT, DFT, DCT, and SVD transformations

Justin Varghese*, Omer Bin Hussain, T Abdul Razak*** and Saudia Subash******

** Karpagam College of Engineering, Coimbatore, Tamil Nadu, India*
***College of Computer Science, King Khalid University, Abha, Saudi Arabia*
****Jamal Mohammed College, Tiruchirapalli, Tamil Nadu, India*
***** Centre for Information Technology & Engineering, Manonmaniam Sundaranar University, India*
** Corresponding Author: justin_var@yahoo.com*

Submitted *:* 30/01/2020
Revised *:* 26/02/2021
Accepted *:* 02/06/2021

ABSTRACT

Digital watermarking provides copyright protection and proof of ownership by inserting watermark metadata as owner's identity in digital documents to prevent authenticity and copyright violations. The paper introduces a new hybrid image watermarking scheme by attaching multiple copies of watermarks in carrier image. The new scheme utilizes the advantages of DWT, DFT, DCT, and SVD transformations to offer stable resistance in protecting watermark contents from various external attacks. The proposed scheme uses Haar wavelet, Fourier, Onion Peel Decomposition, DCT, zigzag ordering, and SVD transformations to decompose the carrier image into four levels to maintain imperceptibility in the watermarked images. The algorithm attaches replicas of watermark frequency blocks in all frequency components of host image to provide better robustness against external deprivations in watermarked images. The proposed algorithm also provides the increased probability of extracting at least one undamaged replica of watermark even when other frequencies are damaged by external attacks. The improved experimental results of the proposed scheme in terms of visual analysis and quantitative metrics on different images with different experimental setup demarcate that the proposed watermarking scheme provides stable performance in generating better watermarked images. It is experimentally found that the new scheme produces high quality watermarked images with an average of 7.62% lesser Mean Absolute Error (MAE) and increased Peak Signal to Noise Ratio (PSNR), Mean Structural Similarity Index Measure (MSSIM), and Feature Similarity Index Measure (FSIM) of 5.02 %, 4.37 %, and 2.37 %, respectively, than the next best algorithms when simulated with 20 sets of watermark and cover images. The watermark images extracted by the proposed algorithm from extremely distorted watermarked images are with better visual and objective values than other methods used in the comparative study. Simulation analysis on 20 sets of watermark and cover images with 30 types of potential attacks reveals that the extracted watermark images through the proposed scheme produces an average of 5.62%, 6.37%, and 5.75% improved Pearson Correlation Coefficients (PCC), Number of Changing Pixel Rate (NPCR), and the Unified Averaged Changed Intensity (UACI) values, respectively, than the next best algorithms used in the comparative study.

Keywords: Copyright protection; Discrete cosine transform; Discrete wavelet transform; Watermarking; Discrete fourier transform; Information security.

INTRODUCTION

The evolution of communication technologies and its widespread use have made the communication of digital documents faster, convenient, and easily accessible (Borra *et al.*, 2018). It has also led to additional vulnerabilities related to counterfeiting, authenticity, integrity, copyright violation, source tracking, broadcast monitoring, ID card security, fraud and tamper detection, content management, etc. Watermarking techniques are developed for maintaining intellectual property/copyright/ownership rights of documents in a cost-effective manner by embedding visible/invisible watermarks as meta-data in the host/owner's documents as authentication identities (Nematollahi *et al.*, 2017; Umamageswari *et al.*, 2014). Digital watermarking techniques help perform transaction tracking, broadcast monitoring, device control, forensics, and content filtering.

Based on the processing in which watermarks are attached, watermarking techniques are grouped into spatial and frequency methods. Spatial domain methods insert watermarks in Least Significant Bit (LSB), altering pixel values of the carrier image (Hussain *et al.*, 2019). Frequency domain methods attach watermark contents in the frequencies of host image rather than attaching directly to the image contents. These methods make the opportunity for selecting suitable frequencies to attach watermark contents, so that the changes due to watermark embedding are not much visible in the host image. Since watermarking techniques in frequency domain embed watermark contents in different frequencies of cover image, these methods show high robustness in protecting watermark from potential attacks than spatial domain techniques. This study proposes a new hybrid watermarking scheme by combining the advantages of DWT, DFT, DCT, and SVD transformations and by attaching multiple copies of watermark contents in carrier image.

RELATED WORKS AND REVIEW

Frequency domain transformations such as DWT, DFT, and DCT decompose the images into different frequency levels and thereby offer watermarking techniques to show better imperceptibility, robustness, security, and capacity by selecting suitable frequency bands to attach watermark contents. Exploiting the advantages of these transformations while embedding watermark contents in the host image, many algorithms (Li *et al*., 2018; Mehta *et al*., 2018; Varghese et al., 2014; Varghese *et al*., 2015; Yadav *et al*., 2018; Sharma *et al.*, 2017; Su *et al.*, 2019; Ganic *et al.*, 2004) evolved by incorporating different frequency transformations. Li J. *et al*. (2018) proposed a Quaternion Hadamard Transform (QHT) based image watermarking scheme. The algorithm creates blocky effects in the watermarked images since it adopts block based processing. The watermarking scheme introduced by Mehta R. *et al*. (2018) uses Genetic Algorithm (GA) and Lagrangian Support Vector Regression (LSVR) in wavelet domain to select specific blocks of host image for attaching watermark contents according to specific regression function. But the algorithm takes more computation time to optimize regression function using GA and LSVR. Varghese J. *et al*. (2015) attached watermark contents in Discrete Cosine Transform (DCT) domain by selecting suitable carrier blocks according to human visual characteristics based on the entropy of different carrier and watermark frequency blocks. B. Yadav (2018) attached watermark contents directly to the singular values of third level Discrete Wavelet transform (DWT). But the extracted watermarks often get destroyed due to external potential attacks since the algorithm attaches watermark contents in the low frequencies alone. Sharma *et al*. (2017) introduced an LSB based watermarking technique that inserts the watermark into the carrier image using LSB and Multiple-Parameter Discrete Fractional Fourier transform (MPDFRFT) for improving robustness. But the execution time required for this proposal is very high. Su Q. *et al*. (2019) introduced spatial domain watermarking procedure by embedding watermark contents in all pixels of the carrier image by quantization; but the watermarked results reflect weak robustness to potential attacks. Hsu, C. S. *et al*. (2019) proposed a watermarking scheme specifically for resisting cropping attacks. Wang, C. *et al*. (2019) used Ternary radial harmonic Fourier moments to hide watermark contents. Najafi, E. & Loukhaoukha, K. (2019) introduced a watermarking scheme by utilizing the advantages of SVD and contourlet

transform. Hu, H. T. et al. (2020) used mixed modulation while attaching watermark contents in carrier images. Thakur, S. et al. (2020) incorporated DWT and SVD hamming code and chaotic encryption to perform encryption during watermark embedding. Ko, H. J. et al. (2020) used interblock correlation to find suitable carrier blocks for attaching watermark contents.

Although these frequency domain methods show improvements in watermarking than spatial domain methods, they find difficulties in retrieving valid watermark contents especially when potential attacks damage the frequencies, where the watermarks are attached. These disadvantages of single copy watermark attachment in specific frequencies are being taken up by other schemes (Ganic *et al*., 2004; Sverdlov *et al*., 2006; Run *et al*., 2012; Varghese *et al*., 2016) to attach multiple watermark replicas in all frequencies to provide better robustness against external deprivations in watermarked images. Watermarks attached in specific frequencies have specific resistance to specific group of attacks, and it varies according to the frequency, where the watermark contents are attached. Hence, if watermark replicas are attached in all frequencies, it is difficult to eliminate or erase the watermark from different frequencies. By attaching replicas of watermark contents at different frequencies of host image, these algorithms always hold higher probability to extract some valid watermark replicas from some host frequencies even when other frequencies are damaged by external attacks. Although these algorithms with multiple watermark replica attachment offer many advantages, their robustness largely depends on the frequency transformations, where different transformations offer different levels of robustness against different external attacks.

When comparing the advantages and disadvantages of major frequency transformations in the field of watermarking, it is identified that DWT provides better spatial-frequency localization of signals due to its inherent multiresolution based basis functions (Poljicak *et al.*, 2011). Due to the wide applications of DCT in JPEG based compression schemes, DCT provides better robustness towards JPEG compression with medium level of energy compaction. Due to the strong sinusoidal properties, Discrete Fourier Transform (DFT) provides robust energy compaction with geometrical invariance properties (Poljicak *et al*., 2011). Hence, many watermarking schemes (Singh, 2017; Navas *et al*., 2008) came up by combining these transformations in watermarking to offer collective resistance towards various potential attacks. But these algorithms suffer the disadvantages of single copy watermark attachment in specific frequencies. Further, these algorithms though combine DCT, DWT, and SVD transformations, they did not take the advantages of DFT or collecting similar frequencies from different subbands to protect watermark contents from external potential attacks.

THE WATERMARKING SCHEME

The new hybrid watermarking algorithm exploits the advantages of DWT, DFT, DCT, and SVD transformations and offers stable resistance in protecting watermark contents from different external attacks without compromising image fidelity and robustness aspects of image watermarking. Since the watermarks attached in specific frequencies have specific resistance to specific group of attacks, the proposed algorithm attaches watermark contents to all frequencies of carrier image. The new hybrid watermarking scheme is outlined in Fig. 1. The new hybrid watermarking algorithm demarcated in Fig. 1 attaches copies of watermark in all frequencies that have extended probability of extracting a valid watermark even from highly impinged watermarked images by external potential attacks than other competing schemes.

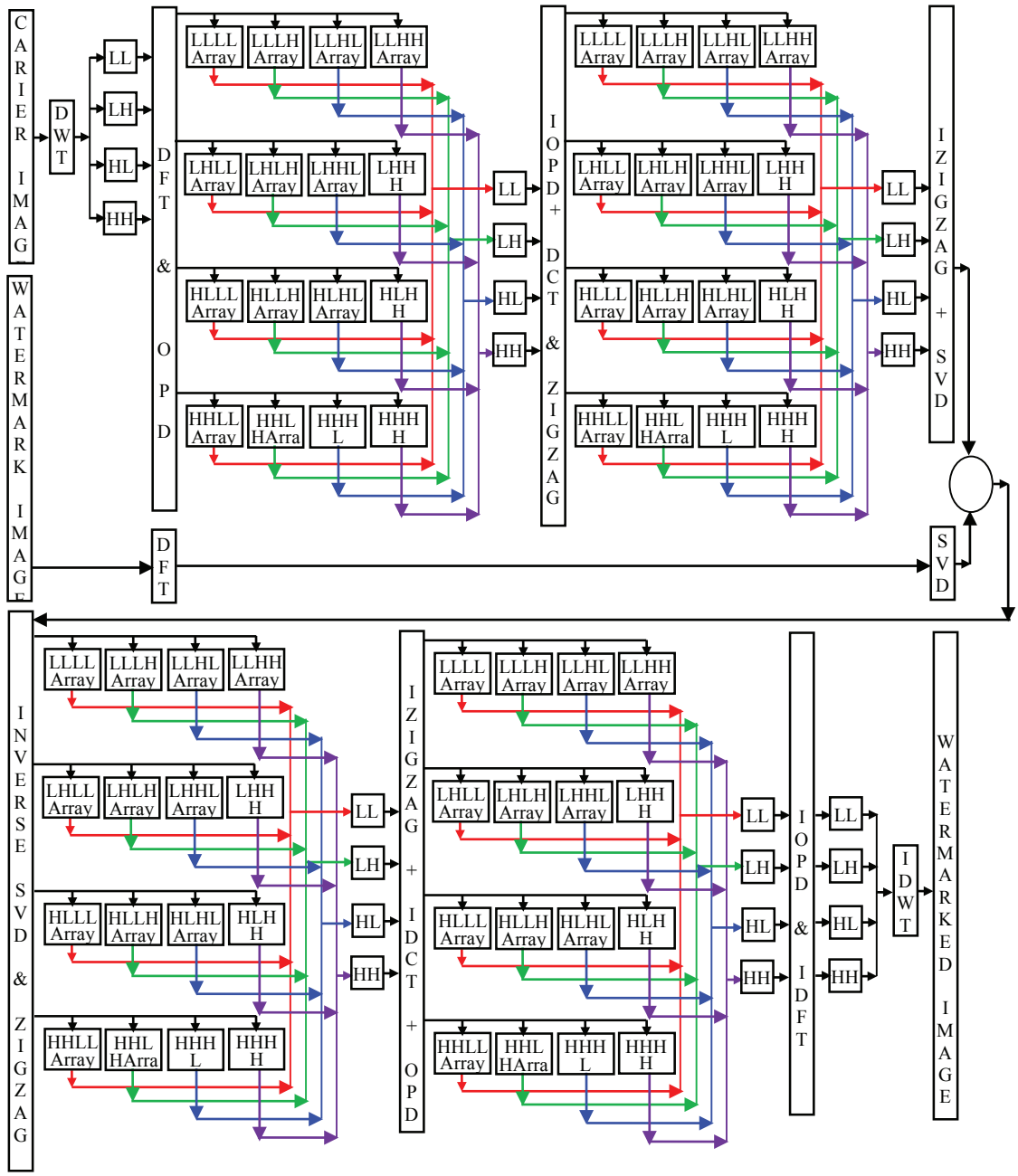

Figure 1. Schematic diagram of new watermarking scheme

At each level of decomposition by different frequency transformations, the new scheme combines similar frequencies from all decomposed frequency subbands before applying next level of decomposition by a different frequency transformation. By combining similar frequency subbands at different levels by different frequency transformations as in Fig. 1, the algorithm provides more robust platform for attaching watermark components. The scheme starts its watermarking process by decomposing the host image with DWT. Further, these algorithms though combine DCT, DWT, and SVD transformations, they did not take the advantages of DFT.

The subsequent sections detail watermark embedding and retrieving stages.

The watermark embedding

The new scheme undergoes four levels of decomposition to maintain imperceptibility qualities in the watermarked images. As in Fig. 1, the algorithm applies Haar wavelet transform and converts the carrier image into Low-Low (LL), Low-High (LH), High-Low (HL), and High-High (HH) frequencies. These frequencies are transformed to second-level frequency decomposition by applying DFT. The Onion Peel Decomposition (OPD) operation (Varghese *et al*., 2016) is applied to these individual frequencies for converting the frequency blocks to corresponding one dimensional array.

From these individual blocks, the corresponding LL, LH, HL, and HH components are separately collected, and the combined arrays are reshaped back to individual blocks by performing Inverse Onion Peel Decomposition (IOPD) operation. As the third level of frequency decomposition, these second-level frequency blocks are further subjected to DCT, and the resultant frequency blocks are reshaped into one-dimensional form by performing zigzag ordering. The LL, LH, HL, and HH components of these individual frequency arrays are separately collected and combined, and the resultant arrays are reshaped back to individual frequency blocks by performing inverse zigzag operation. SVD is finally applied to these frequency blocks as the fourth level frequency decomposition, and the singular values of carrier frequency blocks are combined with singular values of the replicas of watermark frequencies. The algorithm is detailed in the subsequent steps.

Step 1: Since DWT shows spatial-frequency characteristics with localization properties in frequency and time domains, it maintains visible transparency than other transformations (Poljicak, A. *et al*., 2011) by producing high visual qualities in the watermarked images. DWT also offers multiresolution analysis with strong resistance towards noise and contrast based attacks. With the aim of achieving these advantages in the watermarked images, the algorithm applies DWT on carrier image C to create LL, LH, HL, and HH frequency blocks.

Step 2: Fourier transform has strong geometrical invariance properties with high energy compaction capabilities, and it outperforms DWT in protecting watermark contents in case of geometric based external attacks (Poljicak *et al*., 2011). For incorporating these advantages, DFT is applied as a second-level decomposition on LL, LH, HL, and HH subbands of DWT. DFT is performed on watermark image, CW for generating the watermark frequency, W.

Step 3: OPD is a circular traversal applied on Fourier transformed images to decompose frequencies into one-dimensional array, such that the traversal sweeps all frequency components in the order starting from extremely high top left corner to the extremely low Direct Current (DC) frequencies. The algorithm of OPD and its illustration are found in the author's previous work (Varghese *et al.*, 2016). OPD is performed on all Fourier transformed two-dimensional frequency block images to reshape two-dimensional blocks to one-dimensional format devoid of changing the frequency order (Navas *et al*., 2008). For notational convenience, $F_i \ \forall \ i = 1,2, \ldots 4$ denote the Fourier transformed frequency blocks and $\left[FLL_i \ FLH_i \ FHL_i \ FHH_i\right], \ \forall \ i = 1,2, \ldots 4$ denote the resultant blocks of OPD.

Step 4: The proposed scheme groups all similar frequencies from $\left[FLL_i\ FLH_i\ FHL_i\ FHH_i\right]$, $\forall\ i = 1,2,\ldots 4$ arrays as

$$FBl_1 = \bigcup_{i=1}^{4} FLL_i \tag{1}$$

$$FBl_2 = \bigcup_{i=1}^{4} FLH_i \tag{2}$$

$$FBl_3 = \bigcup_{i=1}^{4} FHL_i \tag{3}$$

$$FBl_4 = \bigcup_{i=1}^{4} FHH_i \tag{4}$$

Here, FBl_1, FBl_2, FBl_3 and FBl_4, respectively, denote LL, LH, HL, and HH components of OPD arrays.

Step 5: As the next step, inverse OPD is applied on these one-dimensional arrays FLL, FLH, FHL and FHH to restructure them into two-dimensional blocks B_i, $\forall\ i = 1,2,\ldots 4$ as

$$B_i = IOPD\left(FBl_i\right) \tag{5}$$

Step 6: DCT shows better robustness against JPEG compression and block processing based external attacks (Singh *et al*., 2017), and, hence, DCT is applied as the third level frequency decomposition of the proposed scheme to further decompose the frequency contents of each B_i to D_i, $\forall\ i = 1,2,\ldots 4$.

Step 7: Further, these two-dimensional DCT blocks D_i are converted into one dimension by applying zigzag ordering to collect similar frequencies in the third level decomposition as one-dimensional arrays $\left[DLL_i\ DLH_i\ DHL_i\ DHH_i\right]$, $\forall\ i = 1,2,\ldots 4$.

Step 8: In order to effectively collect the similar frequencies from different frequency blocks in the third level of decomposition, the proposed scheme groups all similar frequencies from arrays $\left[DLL_i\ DLH_i\ DHL_i\ DHH_i\right]$, $\forall\ i = 1,2,\ldots 4$ such that

$$DBl_1 = \bigcup_{i=1}^{4} DLL_i \tag{6}$$

$$DBl_2 = \bigcup_{i=1}^{4} DLH_i \tag{7}$$

$$DBl_3 = \bigcup_{i=1}^{4} DHL_i \tag{8}$$

$$DBl_4 = \bigcup_{i=1}^{4} DHH_i \tag{9}$$

Here, DBl_1, DBl_2, DBl_3 and DBl_4, respectively, denote LL, LH, HL, and HH components of zigzag ordered arrays.

Step 9: In order to apply SVD operation in the proposed scheme, inverse zigzag operation is applied on DBl_1, DBl_2, DBl_3 and DBl_4, respectively, to restructure them into two-dimensional blocks DB_i, $\forall\ i = 1,2,\ldots 4$ as

$$DB_i = izigzag\left(DBl_i\right) \tag{10}$$

Step 10: The singular values of SVD are less affected with external perturbations of cover image, and small changes in singular value contents do not much disturb the image fidelity of the host image (Borra et al., 2011). SVD is individually applied on DWT-DFT-DCT frequency blocks DB_i and watermark frequency block, W to combine the watermark contents in the singular values of carrier frequencies. The SVD operations are given by

$$DB_i = U_i S_i V_i^T \quad \forall\ 1 \le i \le 4 \tag{11}$$

$$W = \overset{w}{U}\ \overset{w}{S}\ \overset{w}{V}^T \tag{12}$$

Here, 'T' is the matrix transpose operation, while U_i, V_i, $\overset{w}{U}$ and $\overset{w}{V}$ are unitary matrices of SVD. Further, S_k and $\overset{w}{S}$ are diagonal matrices with positive real numbers that denote singular value matrices of carrier and watermark frequency blocks, respectively.

Step 11: Once the algorithm has reached four levels of frequency decomposition, the watermark attaching process is performed by combining the cover and watermark singular values. The operation is defined as

$$\tilde{S}_i = S_i + \alpha_i \overset{w}{S} \quad \forall\ 1 \le i \le 4 \tag{13}$$

where α_i denotes the strength parameter, while $\tilde{S}_i$ is the watermarked singular values for the i^{th} carrier frequency block. The strength parameter controls the amount of watermark contents in the watermarked images, and its value highly depends on the application.

Step 12: Once the watermark embedding process is over, the algorithm applies inverse SVD, zigzag ordering, inverse frequency rearrangement, inverse zigzag ordering, inverse DCT, OPD, inverse frequency rearrangement, inverse OPD, inverse DFT, and inverse DWT operations for reconstructing watermarked image, $\tilde{C}$ by performing in order the inverse processes from step 10 to 1.

The watermark extraction

The section details various steps involved in extracting watermark contents from watermarked images. The watermark extraction stage follows the same steps as the embedding scheme but extracts the watermark contents from watermarked images. The subsequent steps detail the watermark extraction process.

Step 1: As the first step of watermark extraction, the algorithm applies steps 1 to 10 of watermark embedding scheme on watermarked image $\tilde{C}^*$ with possible attacks to extract the singular value matrix, $\tilde{S}_i$ from DWT-DFT-DCT frequency blocks $\tilde{DB}_i$. The SVD operation is given by

$$\tilde{DB}_i = \tilde{U}_i \tilde{S}_i \tilde{V}_i^T \quad \forall\ 1 \le k \le 4 \tag{14}$$

where 'T' is the matrix transpose operation, and $\tilde{U}_i$ and $\tilde{V}_i$ are unitary matrices of SVD.

Step 2: Once the algorithm has reached four levels of frequency decomposition, the watermark extraction process is performed for extracting watermark singular values. The operation is defined as

$$\overset{W^*}{S}_i = \frac{\left(\tilde{S}_i - S_i\right)}{\alpha_i} \qquad \forall\ 1 \le i \le 4 \tag{15}$$

where α_i denotes strength parameter, and $\tilde{S}_i$ is the watermarked singular values of the i^{th} frequency block.

Step 3: The algorithm applies inverse SVD to the individual watermark singular values and regenerates the watermark frequency blocks using the extracted singular value replicas as

$$\tilde{W}_i = \overset{w}{U}\ \overset{W^*}{S}_i\ \overset{w'}{V} \tag{16}$$

where α_i denotes strength parameter, and S_i is the watermarked singular values of the i^{th} frequency block.

Step 4: Finally, the watermark image replicas, $\tilde{CW}_i$ are being regenerated by performing the inverse Fourier transform on $\tilde{W}_i$.

Since the proposed scheme combines DWT, DFT, DCT, and SVD transformations in its four level frequency separation and similar frequency collection processes, it not only has the advantage of providing high quality watermarked outputs, but also offers better resistance towards noise, contrast, geometric, JPEG compression, and block based external attacks. Further, by attaching multiple watermark replicas in all frequencies of carrier images, the proposed algorithm provides better chance for extracting at least one undamaged copy of watermark replica even when the potential attack affects other frequencies of watermarked image.

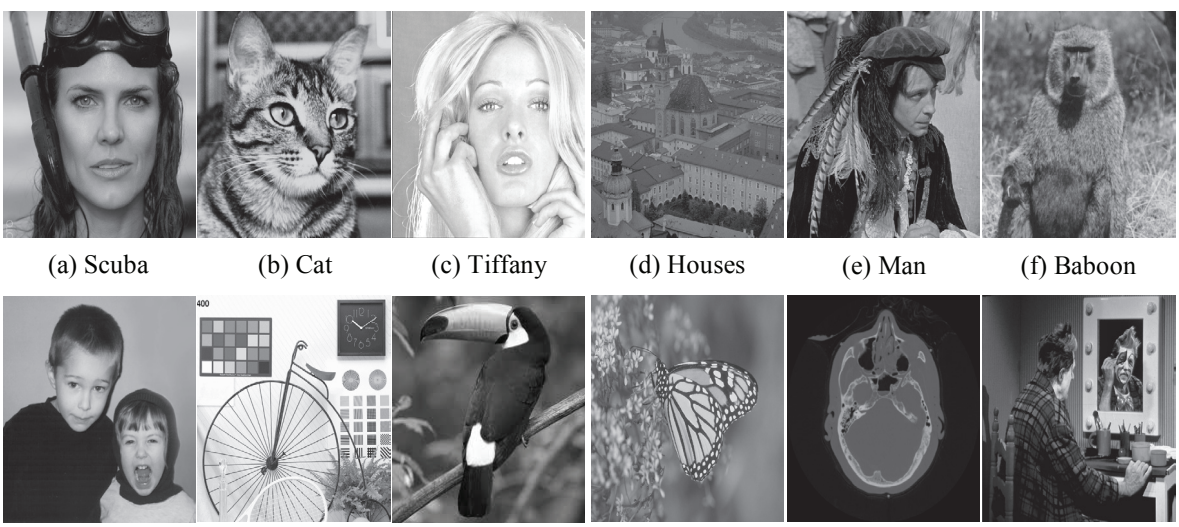

(a) Scuba (b) Cat (c) Tiffany (d) Houses (e) Man (f) Baboon

(g) Boys (h) Bicycle (i) Hornbill (j) Butterfly (k) CTScan (l) Clown

Figure 2. Test images used for experimental analysis as cover ((a) – (f)) and watermark ((g) – (l)) images.

EXPERIMENTAL SIMULATIONS AND ANALYSIS

The experimental simulations presented in this manuscript are made using MATLAB R2014 software in an Intel 3.3 GHz i3 processor 3220 with 4 GB RAM on a 64-bit Windows operating system. Further, the MATLAB code of the new scheme used in this analysis will be made available through https://in.mathworks.com/matlabcentral/profile/authors/17446231 once the paper is published. The image fidelity and robustness of the new watermarking algorithm are analyzed with wide variety of images, of which Scuba, Cat, Tiffany, Houses, Man, Baboon, Boys, Bicycle, Hornbill, Butterfly, CT Scan, and Clown images are discussed in this paper. Fig. 2 shows the test images used in this study. The effectiveness of new watermarking scheme with respect to image fidelity and robustness is performed with Ganic E. *et al*. (2004), Sverdlov A. *et al*. (2006), and Varghese J. *et al*. (2016) algorithms that embed similar replicas of watermark images with similar strength. These algorithms are selected for comparison since they attach the same number of watermark replicas in carrier image frequencies with similar payload. The strength parameter α_i is adjusted for all comparative algorithms for setting equal payload in terms of average pixel wise bitrate of different algorithms.

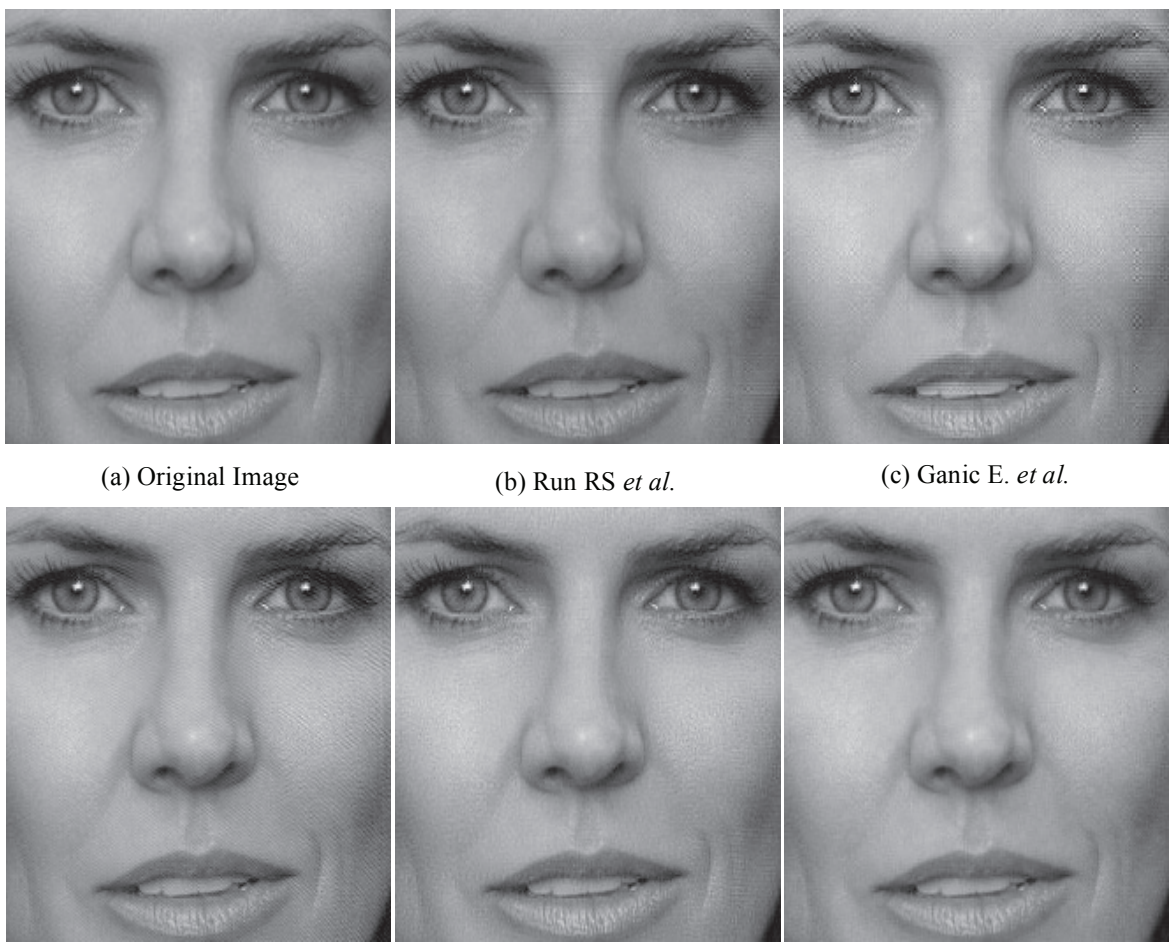

(a) Original Image (b) Run RS *et al.* (c) Ganic E. *et al.*

(d) Sverdlov, A. *et al.* (e) Varghese J *et al.* (f) Proposed Algorithm

Figure 3. Cropped versions of watermarked Scuba images of different algorithms with Boys image as watermark.

Quantitative Metric	Carrier Image	Watermark Image	Algorithms				
			Run R S et al.	Ganic E et al.	Sverdlov A et al.	Varghese J et al.	Proposed Scheme
MAE	Scuba	Boys	6.0163	6.7580	6.8391	4.7128	3.6132
	Cat	Bicycle	10.8120	12.8033	12.8354	6.9695	6.7064
	Tiffany	Hornbill	6.1358	5.3390	6.3186	4.4338	4.1275
	Houses	Butterfly	6.4814	7.4460	7.1886	4.4973	4.3438
	Man	CTScan	2.5933	2.7743	2.7913	1.3169	1.7914
	Baboon	Clown	5.1922	6.5835	5.5203	2.8500	3.0553
PSNR	Scuba	Boys	29.7690	26.6351	26.4987	34.4806	35.4762
	Cat	Bicycle	25.6048	22.3475	22.2479	30.1932	30.2241
	Tiffany	Hornbill	30.4167	28.0459	27.8115	35.3083	35.4112
	Houses	Butterfly	30.2567	27.2532	27.0805	35.1154	35.1696
	Man	CTScan	37.6932	35.3099	34.9682	43.2911	43.2549
	Baboon	Clown	31.9515	29.0001	28.8100	36.8875	36.7502
MSSIM	Scuba	Boys	0.9327	0.9999	0.9999	0.9814	0.9994
	Cat	Bicycle	0.9629	0.9998	0.9998	0.9873	0.9933
	Tiffany	Hornbill	0.9927	1.0000	0.9992	0.9871	0.9973
	Houses	Butterfly	0.9883	0.9999	0.9999	0.9899	0.9983
	Man	CTScan	0.9692	0.9972	0.9962	0.9972	0.9926
	Baboon	Clown	0.9931	0.9753	0.9881	0.9950	0.9988
FSIM	Scuba	Boys	0.9957	0.9685	0.9973	0.9954	0.9984
	Cat	Bicycle	0.9938	0.9571	0.9939	0.9957	0.9978
	Tiffany	Hornbill	0.9947	0.9999	0.9911	0.9964	0.9968
	Houses	Butterfly	0.9936	1.0000	0.9934	0.9971	0.9995
	Man	CTScan	0.9991	1.0000	0.9994	0.9996	0.9998
	Baboon	Clown	0.9959	1.0000	0.9980	0.9983	0.9991

Image fidelity measures the similarity between watermarked and original images, while robustness is the assessment of ability of an algorithm to protect the attached watermarks even in case of extreme potential attacks. An effective watermarking algorithm needs to trade off between robustness and image fidelity. Image fidelity of watermarked images generated by comparative algorithms is evaluated in terms Mean Absolute Error (MAE), Peak Signal to Noise Ratio (PSNR), Mean Structural Similarity Index Measure (MSSIM), and Feature Similarity Index Measure (FSIM). The formulations of PSNR, MSSIM, and FSIM are as denoted in similar papers (Ganic *et al*., 2004; Sverdlov *et al*., 2006; Run *et al*., 2012; Varghese *et al*., 2016).

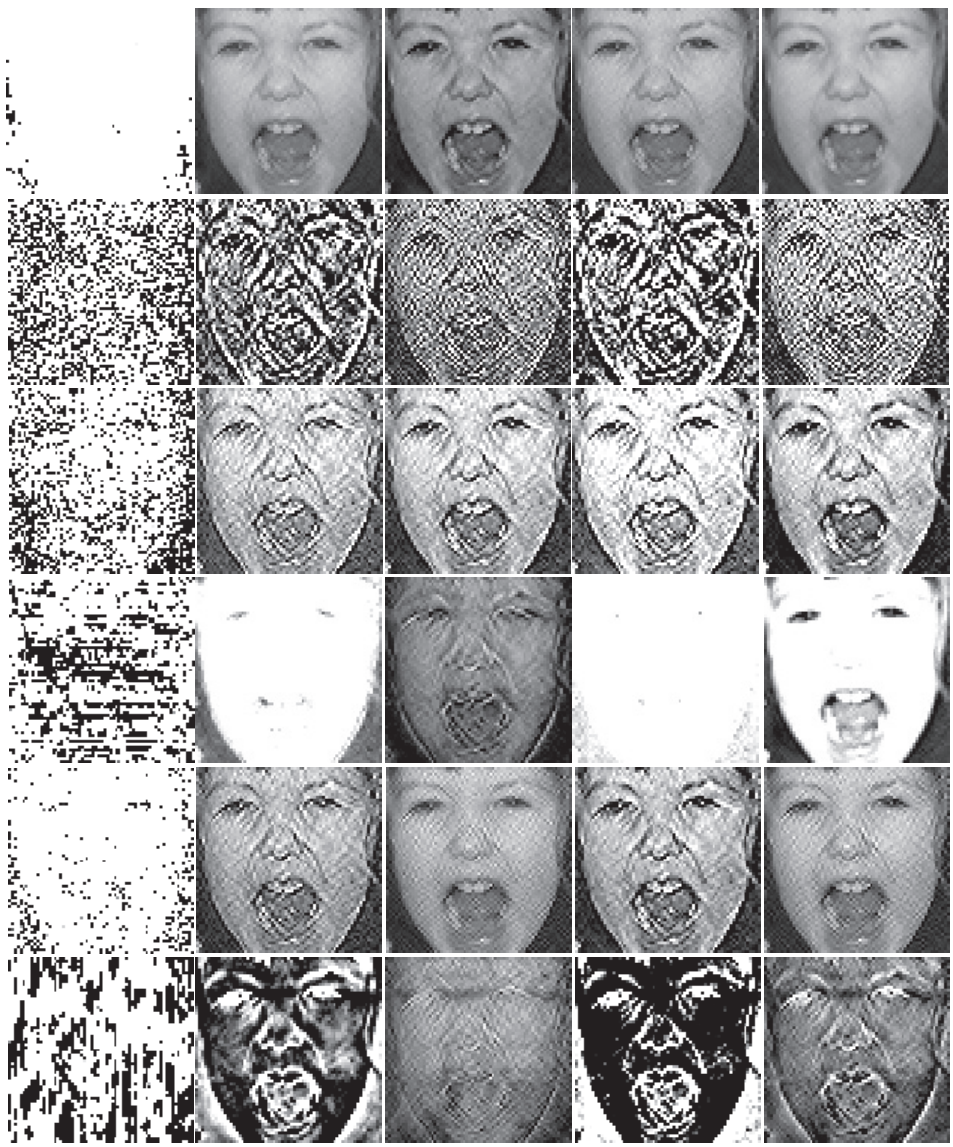

Figure 4. Cropped watermark extracted by comparative schemes from watermarked Scuba image affected by different external attacks: Rows 1-6 are Attacks (Row 1: JPEG80, Row 2: Salt&Pepper05, Row 3: Gaussian Noise02, Row 4: Avg Filter, Row 5: Speckle Noise and Row 6: Motion Blur with Columns 1-5 are different algorithms (Column 1: Run RS et al. 2 , Column 2: Ganic E. et al., Column 3:Sverdlov, A. et al., Column 4: Varghese J et al. Column 5: Proposed scheme)

The cropped versions of watermarked images by comparative schemes are given in Fig. 3. From Fig. 3, it is noted that the watermarked outputs of the new scheme although are closely similar with the outputs produced by Varghese J. *et al*. scheme; it produces better outputs than those of Run RS *et al*., Ganic E. *et al*., Sverdlov A. *et al*. algorithms.

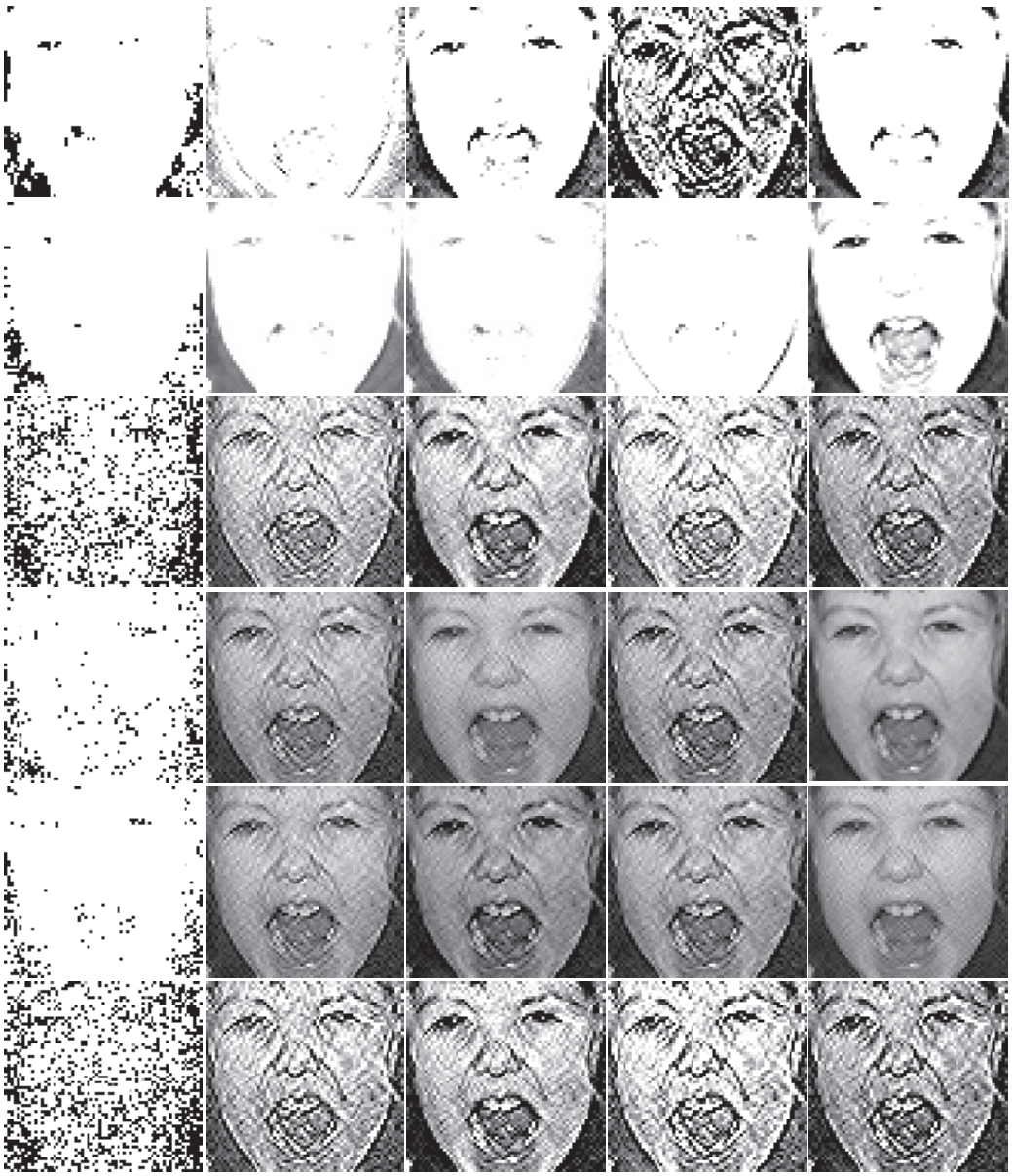

Figure 5. Cropped watermark extracted by comparative schemes from watermarked Scuba image affected by different external attacks: Rows 1-6 are Attacks (Row 1: Unsharp Masking, Row 2: Contrast Stretching, Row 3: JPEG80+Gaussian Noise02, Row 4: JPEG80+SpeckleNoise02, Row 5: JPEG80+Salt&Pepper02 and Row 6: Gaussian Noise 01+Speckle Noise 05 with Columns 1-5 are different algorithms (Column 1: Run RS et al. 2 , Column 2: Ganic E. et al., Column 3:Sverdlov, A. et al., Column 4: Varghese J et al. Column 5: Proposed scheme)

Table 1 makes the MAE, PSNR, MSSIM, and FSIM analysis of watermarked images by comparative schemes. From Table 1, it is visible that the new method has better PSNR, MSSIM, and FSIM with minimum MAE values than Run RS et al., Ganic E. et al., Sverdlov A. et al., and Varghese J. et al. schemes in most of the cases.

Table 2. Objective analysis of extracted Boys watermark from Scuba cover image by various algorithms against different external attacks.

Potential attacks	Ganic E et al.			Sverdlov A et al.			Varghese J et al.			Proposed Scheme		
	PCC	NPCR (%)	UACI (%)	PCC	NPCR (%)	UACI (%)	PCC	NPCR (%)	UACI (%)	PCC	NPCR (%)	UACI (%)I
JPEG with 10% quality	0.993	60.58	11.09	0.997	51.84	10.99	0.996	58.79	9.59	0.997	42.88	3.99
JPEG with 60% quality	0.999	62.94	9.09	0.999	54.95	7.00	0.997	54.84	9.60	0.998	40.92	3.99
JPEG with 100% quality	0.999	59.94	10.09	1.000	57.00	8.00	0.999	56.95	7.60	0.998	43.92	2.99
Impulse Noise 1%	0.877	54.62	12.00	0.962	50.02	8.85	0.795	47.34	10.46	0.975	40.00	6.93
Impulse Noise 5%	0.488	34.28	2.91	0.709	42.87	10.84	0.379	23.71	10.55	0.709	30.36	5.13
Gaussian Noise with 0.01 mean & 0.002 variance	0.955	62.30	4.98	0.955	55.66	11.82	0.948	55.30	11.44	0.970	42.80	6.91
Gaussian Noise with 0.0 mean and 0.001 variance	0.978	61.68	11.06	0.994	57.69	6.98	0.967	55.28	3.58	0.991	41.64	4.97
Gaussian Noise with 0.01 mean and 0.005 variance	0.985	61.10	10.09	0.971	54.49	6.88	0.981	59.01	10.50	0.997	42.88	6.99
Average Filtering 3x3	0.997	64.82	12.09	0.898	48.70	4.59	0.972	55.54	10.23	0.998	43.92	6.99
Gaussian Filtering with 3x3	0.996	65.76	8.10	0.999	52.95	10.00	0.969	50.39	3.60	0.999	43.96	6.00
Median Filtering 3x3	0.987	59.22	10.09	0.998	56.90	6.99	0.917	50.68	11.59	0.997	43.88	4.99
Speckle Noise 0.02	0.829	55.74	8.84	0.926	48.15	7.70	0.723	43.60	10.33	0.936	43.44	6.81
Speckle Noise 0.01	0.928	63.68	5.00	0.972	54.54	9.89	0.881	51.81	9.50	0.975	44.00	2.93
Speckle Noise 0.005	0.971	61.26	4.06	0.990	51.48	6.96	0.960	55.92	11.56	0.991	45.64	6.97
Linear Motion Blurrig 21 pixels, with an angle 11^0	0.469	28.14	8.01	0.942	56.98	4.77	-0.039	0.97	3.39	0.979	42.16	6.94
Unsharp Masking	0.992	64.52	7.07	0.986	55.27	7.94	0.965	57.18	11.55	0.993	40.72	3.98
Image Resizing 512->256	0.990	60.40	9.06	0.997	57.84	11.99	0.885	49.02	10.59	0.990	42.60	2.97
Image Resizing 512->1024	0.999	63.94	5.10	1.000	53.00	10.00	0.998	51.90	4.60	1.000	44.00	7.00
Contrast Stretching	0.999	67.94	12.10	0.999	59.95	12.00	0.972	50.54	3.60	0.999	44.96	3.00
JPEG Compression with 80% quality + Gaussian Noise with 0.01 mean and 0.002 variance	0.951	57.06	9.99	0.951	50.45	5.80	0.940	48.88	8.42	0.973	44.92	3.92
JPEG Compression with 80% quality + Impulse Noise 0.2%	0.984	64.04	12.08	0.996	51.79	11.98	0.974	55.65	5.59	0.995	40.80	6.99
JPEG Compression with 80% quality + Speckle Noise 0.02	0.989	64.34	9.06	0.996	51.79	11.98	0.986	53.27	11.59	0.990	46.60	3.97
Gaussian Noise with 0.01 mean and 0.002 variance + Speckle Noise 0.005	0.921	61.26	10.92	0.932	49.46	11.73	0.902	53.90	11.36	0.956	44.24	2.87
Impulse Noise 0.2+ Speckle Noise 0.005	0.944	64.64	5.05	0.982	53.06	4.93	0.918	53.74	3.54	0.989	41.56	3.97
Histogram Equalization	0.989	62.34	4.08	0.988	59.38	8.95	0.937	49.72	10.56	0.996	47.84	5.99
Pixelate with 2x2 tiles	1.000	67.00	10.10	0.998	56.90	11.99	0.964	57.13	3.59	0.999	43.96	7.00
Pixelate with 4x4 tiles	0.907	59.42	4.08	0.991	56.53	4.96	0.674	36.05	3.57	0.995	44.80	4.99
Column Flipping	1.000	68.00	6.03	0.385	20.02	6.54	0.996	58.79	5.39	0.982	42.28	6.95
Rotation 45^o	0.716	50.96	6.01	0.411	24.37	6.64	0.406	21.11	2.48	0.734	29.36	6.20

Table 3. Objective analysis of extracted Hornbill watermark image from Tiffany cover image by various algorithms against different external attacks.

Potential attacks	Ganic E et al.			Sverdlov A et al.			Varghese J et al.			Proposed Scheme		
	PCC	NPCR (%)	UACI (%)	PCC	NPCR (%)	UACI (%)	PCC	NPCR (%)	UACI (%)	PCC	NPCR (%)	UACI (%)I
JPEG with 10% quality	0.990	61.40	7.05	0.988	57.38	8.95	0.995	53.74	11.56	0.996	39.84	4.99
JPEG with 60% quality	0.997	66.82	6.08	0.996	55.79	3.98	0.998	56.90	7.59	0.998	41.92	5.99
JPEG with 100% quality	0.998	65.88	10.09	0.997	55.84	6.99	0.998	59.90	8.59	0.999	46.96	4.00
Impulse Noise 1%	0.771	52.26	7.89	0.949	52.35	10.80	0.625	39.50	11.42	0.954	46.16	4.86
Impulse Noise 5%	0.457	29.42	7.42	0.591	36.73	6.36	0.386	22.07	8.13	0.597	30.88	3.79
Gaussian Noise with 0.01 mean & 0.002 variance	0.936	62.16	8.94	0.962	50.02	7.85	0.940	56.88	3.46	0.977	41.08	6.93
Gaussian Noise with 0.0 mean and 0.001 variance	0.969	61.14	10.08	0.994	57.69	9.98	0.953	51.56	4.58	0.993	47.72	6.98
Gaussian Noise with 0.01 mean and 0.005 variance	0.981	66.86	12.03	0.983	54.12	5.93	0.975	55.70	5.54	0.997	41.88	6.99
Average Filtering 3x3	0.965	62.90	4.43	0.837	49.52	4.35	0.957	55.76	7.01	0.998	45.92	5.99
Gaussian Filtering with 3x3	0.992	62.52	5.09	0.997	58.84	8.99	0.984	56.17	4.59	0.997	42.88	3.99
Median Filtering 3x3	0.982	63.92	12.07	0.992	55.58	3.97	0.954	53.61	10.57	0.995	44.80	4.99
Speckle Noise 0.02	0.537	34.22	7.03	0.738	44.38	10.95	0.425	24.10	2.66	0.750	36.00	6.25
Speckle Noise 0.01	0.658	43.48	5.65	0.890	47.28	11.56	0.521	30.09	4.20	0.873	36.92	5.62
Speckle Noise 0.005	0.791	49.46	5.94	0.960	50.92	11.84	0.657	35.16	9.46	0.969	38.76	2.91
Linear Motion Blurrig 21 pixels, with an angle 11^0	0.478	30.68	6.70	0.903	52.96	3.61	0.022	3.14	4.25	0.925	40.00	5.78
Unsharp Masking	0.980	65.80	4.87	0.944	50.09	8.78	0.882	47.86	6.40	0.974	46.96	4.92
Image Resizing 512->256	0.980	59.80	4.98	0.970	56.44	4.88	0.902	50.90	4.49	0.987	45.48	4.96
Image Resizing 512->1024	0.999	66.94	8.10	0.999	54.95	8.00	0.998	58.90	5.60	0.999	46.96	5.00
Contrast Stretching	0.875	59.50	9.92	0.957	55.76	3.83	0.835	49.42	10.45	0.926	45.04	2.78
JPEG Compression with 80% quality + Gaussian Noise with 0.01 mean and 0.002 variance	0.933	59.98	4.94	0.961	56.97	5.84	0.942	53.98	10.46	0.961	40.44	6.88
JPEG Compression with 80% quality + Impulse Noise 0.2%	0.979	62.74	9.08	0.996	58.79	8.98	0.976	58.75	6.59	0.995	44.80	3.99
JPEG Compression with 80% quality + Speckle Noise 0.02	0.938	60.28	11.05	0.989	54.43	9.96	0.921	53.89	10.56	0.971	41.84	3.91
Gaussian Noise with 0.01 mean and 0.002 variance + Speckle Noise 0.005	0.708	45.48	5.88	0.947	52.24	3.79	0.677	37.20	11.41	0.935	42.40	3.81
Impulse Noise 0.2+ Speckle Noise 0.005	0.746	46.76	10.85	0.939	49.83	7.76	0.608	34.62	3.38	0.947	38.88	5.84
Histogram Equalization	0.844	56.64	6.81	0.930	56.36	10.72	0.807	45.96	8.35	0.941	45.64	4.82
Pixelate with 2x2 tiles	0.985	65.10	3.94	0.960	53.92	9.84	0.895	46.54	10.46	0.986	40.44	4.96
Pixelate with 4x4 tiles	0.870	56.20	7.73	0.910	50.32	7.64	0.538	35.98	4.28	0.977	45.08	6.93
Column Flipping	1.000	60.00	5.90	0.950	50.40	11.80	0.995	54.74	5.42	0.980	41.20	6.94
Rotation 45^o	0.511	37.66	4.08	0.508	29.42	9.03	-0.148	-2.70	9.83	0.632	28.28	5.90

Table 4. Objective analysis of extracted of extracted Clown watermark image from Baboon cover image by various algorithms against different external attacks.

Potential attacks	Ganic E et al.			Sverdlov A et al.			Varghese J et al.			Proposed Scheme		
	PCC	NPCR (%)	UACI (%)	PCC	NPCR (%)	UACI (%)	PCC	NPCR (%)	UACI (%)	PCC	NPCR (%)	UACI (%)I
JPEG with 10% quality	0.565	40.90	5.08	0.994	51.69	10.98	0.992	58.58	10.58	0.996	46.84	3.99
JPEG with 60% quality	0.718	45.08	9.10	0.999	55.95	11.00	0.998	52.90	7.60	0.999	46.96	5.00
JPEG with 100% quality	0.999	66.94	7.10	1.000	53.00	11.00	1.000	56.00	3.60	1.000	46.00	6.00
Impulse Noise 1%	0.543	34.58	4.95	0.963	56.08	7.85	0.788	47.98	9.47	0.961	38.44	3.88
Impulse Noise 5%	0.223	17.38	7.01	0.734	42.17	10.94	0.430	30.36	9.64	0.862	37.48	4.59
Gaussian Noise with 0.01 mean & 0.002 variance	0.393	23.58	11.85	0.940	49.88	3.76	0.942	53.98	8.38	0.962	42.48	6.89
Gaussian Noise with 0.0 mean and 0.001 variance	0.754	47.24	7.03	0.984	54.17	4.94	0.951	53.45	3.54	0.986	45.44	3.96
Gaussian Noise with 0.01 mean and 0.005 variance	0.629	37.74	8.96	0.966	51.23	5.86	0.971	50.49	7.48	0.997	44.88	3.99
Average Filtering 3x3	0.103	12.18	4.18	0.776	40.35	9.10	0.953	56.56	6.79	0.996	47.84	5.99
Gaussian Filtering with 3x3	0.963	57.78	9.07	0.992	59.58	8.97	0.928	56.26	11.57	0.995	40.80	6.99
Median Filtering 3x3	0.852	52.12	10.94	0.961	55.97	7.84	0.767	41.88	8.46	0.976	45.04	3.93
Speckle Noise 0.02	0.522	34.32	11.90	0.952	51.50	10.81	0.708	39.82	3.43	0.894	40.76	2.68
Speckle Noise 0.01	0.654	44.24	4.91	0.953	53.56	6.81	0.862	52.82	8.43	0.957	41.28	4.87
Speckle Noise 0.005	0.774	51.44	9.95	0.964	56.13	3.86	0.952	57.50	4.47	0.985	42.40	5.96
Linear Motion Blurrig 21 pixels, with an angle 11^0	0.298	25.88	5.61	0.637	35.12	4.55	-0.164	8.53	5.29	0.688	35.52	2.06
Unsharp Masking	0.812	54.72	6.85	0.940	52.88	3.76	0.903	50.96	6.38	0.941	37.64	3.82
Image Resizing 512->256	0.816	54.96	3.98	0.971	57.49	9.88	0.792	41.18	11.50	0.975	43.00	4.93
Image Resizing 512->1024	0.893	59.58	7.10	0.999	55.95	9.00	0.996	58.79	7.60	0.999	41.96	5.00
Contrast Stretching	0.759	51.54	6.08	0.995	53.74	5.98	0.993	52.64	8.58	0.985	41.40	3.96
JPEG Compression with 80% quality + Gaussian Noise with 0.01 mean and 0.002 variance	0.395	26.70	8.85	0.938	54.78	6.75	0.937	51.72	3.38	0.939	38.56	5.82
JPEG Compression with 80% quality + Impulse Noise 0.2%	0.806	48.36	7.01	0.978	56.86	9.91	0.975	55.70	10.52	0.982	47.28	3.95
JPEG Compression with 80% quality + Speckle Noise 0.02	0.861	53.66	11.05	0.988	52.38	9.95	0.984	52.17	7.56	0.989	43.56	4.97
Gaussian Noise with 0.01 mean and 0.002 variance + Speckle Noise 0.005	0.330	24.80	6.79	0.925	51.10	5.70	0.903	52.96	6.33	0.918	43.72	4.75
Impulse Noise 0.2+ Speckle Noise 0.005	0.686	42.16	11.93	0.958	51.82	10.83	0.904	53.01	11.45	0.972	38.88	3.92
Histogram Equalization	0.872	60.32	7.98	0.971	55.49	3.88	0.965	57.18	5.50	0.973	46.92	5.92
Pixelate with 2x2 tiles	0.654	43.24	12.07	0.993	54.64	7.97	0.966	51.23	11.57	0.995	40.80	6.99
Pixelate with 4x4 tiles	0.482	36.92	8.01	0.977	53.80	7.91	0.479	25.91	10.52	0.969	38.76	5.91
Column Flipping	0.277	23.62	9.89	0.462	31.02	4.85	0.946	51.19	5.66	0.959	40.36	5.88
Rotation 45^o	0.564	37.84	9.33	0.568	33.54	2.27	0.594	31.89	3.04	0.586	25.44	2.76

Robustness analysis of different algorithms is performed in terms of Pearson's Correlation coefficient (PCC), Number of Changing Pixel Rate (NPCR), and the Unified Averaged Changed Intensity (UACI) (Wu, Y. et al., 2011). PCC quantifies the linear associative relationship between singular values of original and the extracted watermarks (Poljicak *et al*., 2011). PCC outcome varies from +1 to −1. If PCC outcome is +1, it indicates maximum positive linear correlation, while 0 indicates noncorrelation among two singular value matrices. Also, −1 indicates a highly negative linear correlation showing large deviation between the singular values of the original and extracted watermarks. For conducting effective comparison of all algorithms, the best PCC values from all watermark replicas are used for assessing the robustness of all algorithms used in the study. In cryptography, NPCR/UACI scores are usually used for analyzing the resistance of cipher images to the changes in pixels of plain images. The Number of Changing Pixel Rate (NPCR) and the Unified Averaged Changed Intensity (UACI) determine the robustness of image watermarking against external potential attacks. Although higher NPCR/UACI score normally shows higher resistance to differential attacks in the case of cipher and plain texts, but for watermarking, a lower NPCR/UACI score indicates higher robustness of watermarking schemes against external potential attacks. If CW and $\tilde{CW}$ denote the original and the extracted watermarks, the NCPR is defined as

$$NCPR = \frac{\sum_{i=1}^{M}\sum_{j=1}^{N} D(i,j)}{M \times N} \times 100 \quad (\%) \tag{17}$$

where

$$D(i,j) = \begin{cases} 1 & if \ CW(i,j) = \tilde{CW}(i,j) \\ 0 & Otherwise \end{cases} \tag{18}$$

The UACI is defined by

$$UACI = \frac{\sum_{i=1}^{M}\sum_{j=1}^{N} \left| CW(i,j) - \tilde{CW}(i,j) \right|}{M \times N * 255} \times 100 \quad (\%) \tag{19}$$

The average bitrate for all algorithms is kept constant to analyze the robustness of all algorithms. The external attacks used for analyzing the robustness of different algorithms are JPEG, impulse noise, Gaussian noise, average filtering, Gaussian filtering, median filtering, speckle noise, motion blurring, unsharp masking, image resizing, contrast stretching, histogram equalization, pixelate, flipping, and rotation. PCC, NPCR, and UACI values of different algorithms obtained for different watermark and carrier images damaged with various potential attacks are presented in Table 2 to Table 4.

From Table 2 to Table 4, it is found that the new algorithm is consistent in its performance for majority of attacks. The higher PCC with lower NPCR and UACI values produced by the proposed scheme for most of the

external attacks demarcate the consistency and improved performance of new scheme over other comparative algorithms used in the experimental study. Fig. 4 and 5 show the cropped versions of extracted Boys watermarks produced by Run RS *et al*., Ganic E. *et al*., Sverdlov A. *et al*., Varghese J. *et al*. and the proposed algorithms from watermarked Scuba images. From Fig. 4 and 5, it is clear that the new scheme is effective in resisting JPEG80, speckle noise, and filtering based potential attacks, while its performance is moderate against Gaussian noise and contrast stretching based potential attacks.

CONCLUSION

The paper introduced a new watermarking algorithm by attaching replicas of watermark contents in carrier image by combining the advantages of DWT, DFT, DCT, and SVD transformations. As the proposed algorithm attaches multiple replicas in different frequencies of host image, the proposed algorithm provided more opportunity to extract at least some undamaged copies of watermark when potential attacks affect other attached frequencies. By combining similar frequency subbands at different levels using different frequency transformations, the algorithm refines the frequency bands and thereby paves the way for providing better robustness for attaching watermark components in case of potential attacks. Image fidelity of watermarked images generated by comparative algorithms is evaluated in terms MAE, PSNR, MSSIM, and FSIM. The experimental analysis based on visual and quantitative metrics such as NPCR and UACI with wide set of test images showed that the robustness of the new scheme is consistent for all attacks, and it provided better visual output with improved quantitative metrics than other comparative algorithms for most of the external attacks.

REFERENCES

Borra, S., Thanki, R., & Dey, N. 2018. Digital image watermarking: theoretical and computational advances. CRC Press.

Ganic, E., & Eskicioglu, A. M. 2004, September. Robust DWT-SVD domain image watermarking: embedding data in all frequencies. In Proceedings of the 2004 Workshop on Multimedia and Security (pp. 166-174). ACM.

Hsu, C. S., & Tu, S. F. 2019. Enhancing the robustness of image watermarking against cropping attacks with dual watermarks. Multimedia Tools and Applications, 1-27.

Hu, H. T., Hsu, L. Y., & Chou, H. H. 2020. An improved SVD-based blind color image watermarking algorithm with mixed modulation incorporated. Information Sciences.

Hussain, O. B., Razak, A., & Varghese, J. 2019. Comparative Analysis of Prominent Watermarking Algorithms. In Innovations in Computer Science and Engineering (pp. 361-369). Springer, Singapore.

Ko, H. J., Huang, C. T., Horng, G., & Shiuh-Jeng, W. A. N. G. 2020. Robust and blind image watermarking in DCT domain using inter-block coefficient correlation. Information Sciences, 517, 128-147.

Li, J., Yu, C., Gupta, B. B., & Ren, X. 2018. Color image watermarking scheme based on quaternion Hadamard transform and Schur decomposition. Multimedia tools and applications, 77(4), 4545-4561.

Mehta, R., Rajpal, N., & Vishwakarma, V. P. 2018. Robust image watermarking scheme in lifting wavelet domain using GA-LSVR hybridization. International Journal of Machine Learning and Cybernetics, 9(1), 145-161.

Najafi, E., & Loukhaoukha, K. 2019. Hybrid secure and robust image watermarking scheme based on SVD and sharp frequency localized contourlet transform. Journal of information security and applications, 44, 144-156.

Navas, K. A., Ajay, M. C., Lekshmi, M., Archana, T. S., & Sasikumar, M. 2008, January. Dwt-dct-svd based watermarking. In 2008 3rd International Conference on Communication Systems Software and Middleware and Workshops (COMSWARE'08) (pp. 271-274). IEEE.

Nematollahi, M. A., Vorakulpipat, C., & Rosales, H. G. 2017. Digital watermarking. Springer Singapore.

Poljicak, A., Mandic, L., & Agic, D. 2011. Discrete Fourier transform-based watermarking method with an optimal implementation radius. Journal of Electronic Imaging, 20(3), 033008.

Run, R. S., Horng, S. J., Lai, J. L., Kao, T. W., & Chen, R. J. 2012. An improved SVD-based watermarking technique for copyright protection. Expert Systems with applications, 39(1), 673-689.

Sharma, D., Saxena, R., & Singh, N. 2017. Dual domain robust watermarking scheme using random DFRFT and least significant bit technique. Multimedia Tools and Applications, 76(3), 3921-3942.

Singh, A. K. 2017. Improved hybrid algorithm for robust and imperceptible multiple watermarking using digital images. Multimedia Tools and Applications, 76(6), 8881-8900.

Su, Q., Liu, D., Yuan, Z., Wang, G., Zhang, X., Chen, B., & Yao, T. 2019. New Rapid and Robust Color Image Watermarking Technique in Spatial Domain. IEEE Access, 7, 30398-30409.

Sverdlov, A., Dexter, S., & Eskicioglu, A. M. 2006. Secure DCT-SVD domain image watermarking: embedding data in all frequencies. In Image Processing Seminar at Brooklyn College, NY.

Thakur, S., Singh, A. K., Kumar, B., & Ghrera, S. P. 2020. Improved DWT-SVD-Based Medical Image Watermarking Through Hamming Code and Chaotic Encryption. In Advances in VLSI, Communication, and Signal Processing (pp. 897-905). Springer, Singapore.

Umamageswari, A., & Suresh, G. R. 2014. Secure medical image communication using ROI based lossless watermarking and novel digital signature. Journal of Engineering Research, 3(2), 1-22.

Varghese, J., Subash, S., Hussain, O. B., Nallaperumal, K., Saady, M. R., & Khan, M. S. 2016. An improved digital image watermarking scheme using the discrete Fourier transform and singular value decomposition. Turkish Journal of Electrical Engineering & Computer Sciences, 24(5), 3432-3447.

Varghese, J., Subash, S., Hussain, O. B., Saady, M. R., Babu, B., & Riazuddin, M. 2015. Image adaptive DCT-SVD based digital watermarking scheme by human visual characteristics. Journal of Engineering Research, 1(3), 1-18.

Varghese, J., Omer B. H., Bijoy B., Jamshid M. B., Saudia S., Mohamed R. S., and Mohamed S. K.. 2014. An efficient DCT-SVD based algorithm for digital image watermarking. In 2014 International Carnahan Conference on Security Technology (ICCST), (pp. 1-6). IEEE.

Wang, C., Wang, X., Xia, Z., & Zhang, C. 2019. Ternary radial harmonic Fourier moments based robust stereo image zero-watermarking algorithm. Information Sciences, 470, 109-120.

Wu, Y., Noonan, J. P., & Agaian, S. 2011. NPCR and UACI randomness tests for image encryption. Cyber journals Multidisciplinary journals in science and technology, Journal of Selected Areas Telecommunications (JSAT), 1, (2), 31–38.

Yadav, B., Kumar, A., & Kumar, Y. 2018. A robust digital image watermarking algorithm using DWT and SVD. In Soft Computing: Theories and Applications (pp. 25-36). Springer, Singapore.